

# Nanoscale

Accepted Manuscript



This is an *Accepted Manuscript*, which has been through the Royal Society of Chemistry peer review process and has been accepted for publication.

*Accepted Manuscripts* are published online shortly after acceptance, before technical editing, formatting and proof reading. Using this free service, authors can make their results available to the community, in citable form, before we publish the edited article. We will replace this *Accepted Manuscript* with the edited and formatted *Advance Article* as soon as it is available.

You can find more information about *Accepted Manuscripts* in the [Information for Authors](#).

Please note that technical editing may introduce minor changes to the text and/or graphics, which may alter content. The journal's standard [Terms & Conditions](#) and the [Ethical guidelines](#) still apply. In no event shall the Royal Society of Chemistry be held responsible for any errors or omissions in this *Accepted Manuscript* or any consequences arising from the use of any information it contains.

## Minireview

# Perovskite Photovoltaics: A High-Efficiency Newcomer to Solar Cell Family

Cite this: DOI: 10.1039/x0xx00000x

Baohua Wang, Xudong Xiao\* and Tao Chen\*

Received 00th January 2012,

Accepted 00th January 2012

DOI: 10.1039/x0xx00000x

www.rsc.org/

Organometal trihalide perovskite-based light absorbers have attracted great attention due to the excellent photovoltaic properties. The swift development in the device fabrication techniques has led to the power conversion efficiencies exceeding 17%. In this minireview, we will present the typical characteristics of the materials and device structures, followed by analysing updated understandings on the operational principles of the devices. We will also point out the outstanding issues regarding the materials and devices. Finally, as a high-efficiency newcomer to solar cell family, we will discuss its potential impact on the relevant photovoltaics.

## 1. Introduction

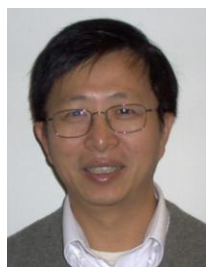
Mankind has been heavily and extensively relying on the fossil fuels for power in daily life, while it is increasingly acknowledged that the burning of fossil fuels would cause deterioration of environment such as greenhouse effect, heavy haze, and air and water pollution. Furthermore, a horrible prediction is that the three main types of fossil fuels, nature gas, coal and oil, will be consecutively exhausted in the next few decades. Therefore, to find sufficient alternative energy sources is an urgent task for a sustainable world. Conversion of solar energy into electricity by photovoltaic solar cell is one of the most promising approaches to cope with energy shortage. First, the energy irradiated from the sun to earth is around 10,000 times of the human energy consumption rate.<sup>1</sup> Second, the radiant energy is virtually inexhaustible and free of charge for human use. Third, the energy conversion by photovoltaic solar cell is featured as clean and safe.

It is generally accepted that, for the application of solar cells

in residential system, the devices have to possess three characteristics: high-efficiency, low-cost in terms of materials, fabrication technique, solar panel installation, and long-term stability. Unfortunately, to date there has been no such a kind of device that can simultaneously meet the requirements. The first two generation solar cells are of high efficiency and long-term stability. However, they also possess some disadvantages. For instance, the high-efficiency silicon solar cell usually requires high cost purification process. The scarcity of indium is a potential challenge for widespread use of CIGS solar cell. The toxic Cd and low earth abundance Te are often regarded as the disadvantages of CdTe solar cells. To develop solar cells that can meet the so-called “golden triangle” requirements, people have made continuous efforts into the creation of new device structures as well as exploitation of new light absorbing materials.<sup>2</sup> The new (third) generation solar cells are primarily associated with nanotechnology. The typical devices are dye-sensitized solar cells (DSSCs) and organic solar cell (OPV) or



Dr. Tao Chen is currently a research assistant professor at the department of physics, the Chinese University of Hong Kong. He received his B.E. degree from Anhui University of Science and Technology, M.Sc. degree from the University of Science and Technology of China in 2007 and Ph.D. degree in Chemistry at Nanyang Technological University (Singapore) in 2010. He joined the Chinese University of Hong Kong in 2011. His research interests include materials, science, fabrication and engineering of organic/inorganic hybrid solar cells.



Professor Xudong Xiao received his Ph. D. degree in physics at the University of California at Berkeley in 1992. He joined the Chinese University of Hong Kong in 2007 and became the founding director of Photovoltaic Solar Energy in Shenzhen Institute of Advanced Technology in 2008. His areas of interest include surface science, nano science and renewable energy science and engineering. In addition to the lab device fabrication and physics study of various thin film solar cells, Prof. Xiao is also leading a team to develop instrumentation and production lines for manufacture Cu(InGa)Se<sub>2</sub> thin film solar panels in China.

polymer solar cells (PSCs) which have gained substantial attraction and improvement in the past decades.<sup>3-5</sup> In contrast to the vacuum deposition method for conventional thin film devices, most of the fabrication steps for new generation solar cells are based on solution processed methods. This is considered as one of the most significant attractive characteristics regarding the reduction of fabrication cost. Since the discovery, tremendous efforts have been devoted to the investigation of the basic operational principles and improvement of solar-to-electrical power conversion efficiency (PCE).<sup>6-12</sup> The record PCEs of DSSCs and PSCs have been boosted to 13% and 11%, respectively.<sup>2,13</sup> Considering that the PCE is the main driver of the cost for the solar cells, obviously, further enhancement in the efficiencies are required.

The PCE improvement is substantially dependent on the light absorbing material; it sets the threshold for the final PCE. This is evidenced by the fact that the state-of-the-art efficiencies were mostly achieved in newly developed absorber materials, such as various dye molecules,<sup>12-14</sup> quantum dots<sup>15,16</sup> and semiconducting polymers.<sup>2,17-19</sup> The most recent development in the organometal trihalide perovskite (such as  $\text{CH}_3\text{NH}_3\text{PbI}_3$ ) based solar cells upgrades the third generation solar device from both material and architecture perspectives. The certified efficiency has reached 17.9%.<sup>2</sup> It is comparable to the traditional thin film solar cells such as those based on CIGS and CdTe light absorbers.

Organic-inorganic hybrid perovskite  $\text{CH}_3\text{NH}_3\text{PbX}_3$  ( $X = \text{Br}, \text{I}$ ) was initially utilized as light absorber in 2009 by Miyasaka and co-workers.<sup>20</sup> This pioneer work was conducted by absorbing the perovskite onto  $\text{TiO}_2$  surface in conventional DSSC structures. However, due to the low surface coverage of the perovskite absorber and the corrosive liquid electrolyte, the advantage of the absorber material did not stand out. The PCEs were only 3.81% for triiodide and 3.13% for tribromide based perovskite sensitizers. By optimizing the surface of  $\text{TiO}_2$  nanoparticle surface and increasing the loading capacity of the perovskite, in 2011, Park et al. achieved 6.5% efficiency under one sun illumination.<sup>21</sup> It was also noted that the perovskite is quite easy to be dissolved in the liquid electrolyte, which causes serious damage on the device. The lifetime of the device lasts only several minutes. Using solid-state hole transporting materials (HTM) and increasing the loading capacity of the perovskite materials significantly improved the efficiency. In 2012, Park, Grätzel and coworkers utilized 2,2',7,7'-tetrakis-(*N,N*-dimethoxyphenyl-amine)-9,9'-spirobifluorene (spiro-MeOTAD) as solid state HTM, generating an efficiency of 9.7%.<sup>22</sup> The device is based on mesoporous  $\text{TiO}_2$  nanoparticles supported  $\text{CH}_3\text{NH}_3\text{PbI}_3$ . Later on, Snaith et al. applied  $\text{Al}_2\text{O}_3$  as scaffold to replace the  $\text{TiO}_2$ . It is believed that  $\text{Al}_2\text{O}_3$  can significantly reduce the loss of voltage.<sup>23</sup> This device structure leads to an open circuit voltage of 1.13 V and PCE of 10.9%. Subsequently, the efficiency was improved to around 15% by two typical device structures based on planar heterojunction and mesoporous  $\text{TiO}_2$  network.<sup>24,25</sup> The research enthusiasm of



Mr. Baohua Wang obtained his B.S. degree in physics at Fudan University in 2011. He is now a Ph.D. student with Dr. Tao Chen at The Chinese University of Hong Kong. His research interests include the preparation of stable and reproducible perovskite film and probing the chemical and physical processes of the materials and devices.

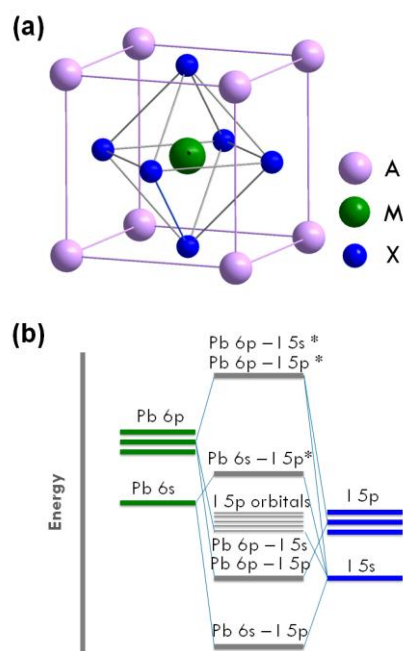


**Fig. 1** (a) Crystal structure of organometal perovskite  $\text{AMX}_3$  with cubic symmetry, in which A is located at the corner of the cube, M is in the centre of the octahedron and X is in the corner of the octahedron. (b) Energy diagram of  $[\text{PbI}_6]^{4-}$  cluster (zero-dimensional system). (b) is adapted by permission from ref. 28.

the perovskite solar cell was thus fuelled and fanned by the highly achievable efficiency, during which a number of perovskite materials, device configurations and fabrication techniques were investigated for comprehensively improving the device performance.

## 2. Crystal and band structure of organic-inorganic hybrid perovskite

Broadly speaking, organic-inorganic hybrid perovskite can be described as  $(\text{RNH}_3)_2(\text{CH}_3\text{NH}_3)_{n-1}\text{M}_n\text{I}_{3n+1}$ , where  $R = \text{alkyl, phenethyl, etc.}$ ;  $M = \text{Pb, Sn}$ ;  $n = 1, 2, \dots, \infty$ . The inorganic and organic layers are stacked in an alternate manner. The inorganic layers are in-plane covalently bonded, while van der Waals force between the organic layers exists perpendicularly to the inorganic layer. This perovskite structure usually forms quantum well like layered structures. The band gap of this multi-layer hybrid perovskite is usually larger than 2 eV.<sup>26</sup>

Once the size of organic cation is reduced, the structure would evolve from the original tetragonal symmetric structure to cubic symmetry. The increased symmetry can lead to a decrease of the band gap. For example, the band gap of archetypal hybrid perovskite  $\text{CH}_3\text{NH}_3\text{PbI}_3$  is around 1.5 eV. This type of cubic organic-inorganic hybrid perovskites generally adopt chemical structure as  $\text{AMX}_3$ , in which A locates at the corner of the cubes, M is at the centre and X is monovalent anion in the centre of the six planes (Fig. 1a). The formation of perovskite is estimated by a tolerance factor ( $t$ ) which is associated with the radii of the A, M and X:<sup>27</sup>

$$t = \frac{R_A + R_X}{\sqrt{2}(R_M + R_X)}$$

where  $R_A$ ,  $R_M$  and  $R_X$  are radii of A, M and X. In addition, another factor  $\mu$  is defined as the ratio  $R_M/R_X$  which can also

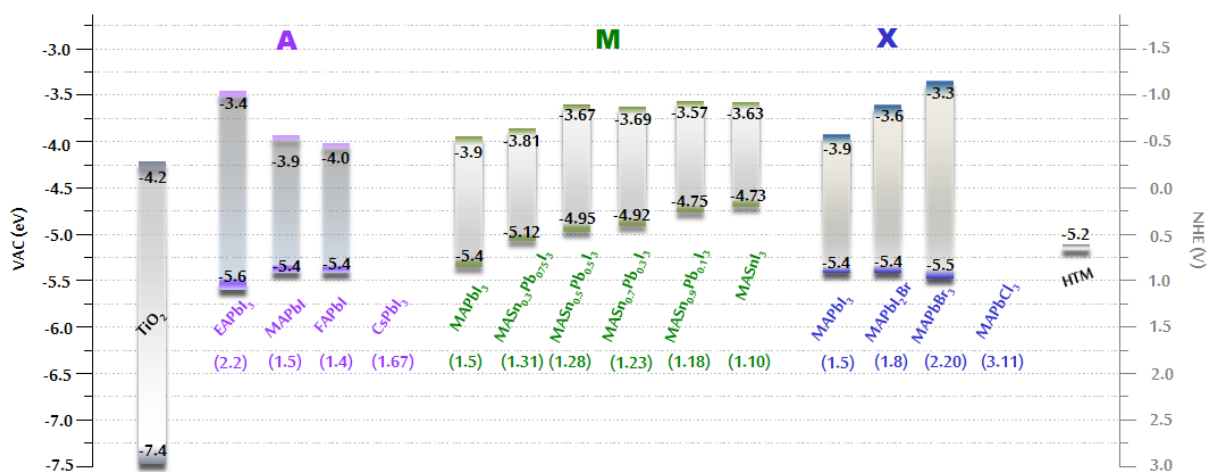


**Figure 2.** Energy levels vs. vacuum and NHE for various perovskite absorbers, TiO<sub>2</sub> and a conventional hole transporting material, 2,2',7,7'-tetrakis-(*N,N*-dimethoxyphenyl-amine)-9,9'-spirobifluorene (spiro-MeOTAD). For the MAPbCl<sub>3</sub>, there is no reference regarding the band structures. MA = CH<sub>3</sub>NH<sub>3</sub><sup>+</sup>, EA = CH<sub>3</sub>CH<sub>2</sub>NH<sub>3</sub><sup>+</sup>, FA = NH<sub>2</sub>-CH=NH<sub>3</sub><sup>+</sup>. The references of each value are provided in the text wherever mentioned. The values under the chemical formula are the corresponding band gap, in eV. There are only bandgap values of CsPbI<sub>3</sub> and MAPbCl<sub>3</sub> are found, the valence and conduction band edges were not found in literature.

influence the crystal structure. Generally, the crystallographic stability and an octahedral inorganic MX<sub>6</sub> can be generated as cubic perovskite when  $0.89 < t < 1.0$  and  $0.44 < \mu < 0.90$ . With this flexibility, a number of elements can serve as substituents for the perovskite light absorbing materials.

The band structure of the perovskite is primarily dependent on the inorganic components. For example, in CH<sub>3</sub>NH<sub>3</sub>PbI<sub>3</sub>, its valence band maxima originates from  $\sigma$  bonding orbital composed of Pb 6s – I 5p (Fig. 1b). The conduction band minima is consisted of Pb 6p – I 5s  $\sigma$  and Pb 6p – I 5p  $\pi$  antibonding orbitals.<sup>28</sup> Therefore, the band gap is mainly determined by the [PbI<sub>6</sub>]<sup>4-</sup>, which is also confirmed by the first principle modelling.<sup>29</sup> According to the Schockely-Queisser limit curve for single junction solar cells, the most suitable band gap of the light absorbing material is 1.4 eV.<sup>30</sup> On the other hand, in order to fabricate colourful solar panels for building-integrated photovoltaics (BIPV), a series of organic molecules and atoms have been applied to tailor the band gap.

### 2.1 The influence of A on the optical properties of APbI<sub>3</sub>

In cubic perovskite structures, although the A position does not significantly influence the band structures, the alternation on A can still tailor the band structure to a small extent. Actually, the band structure of CH<sub>3</sub>NH<sub>3</sub>PbI<sub>3</sub> is close to the optimum value. This small alternation is able to tune the band gap for the optimum value. To narrow down the band gap of CH<sub>3</sub>NH<sub>3</sub>PbI<sub>3</sub>, NH<sub>2</sub>-CH=NH<sub>2</sub><sup>+</sup> (FA), a similar organic component to CH<sub>3</sub>NH<sub>3</sub><sup>+</sup> has been utilized for the perovskite absorbers, forming NH<sub>2</sub>-CH=NH<sub>2</sub>PbI<sub>3</sub> with band gap of 1.4 eV.<sup>31</sup> The device based on this perovskite exhibits significantly extended photocurrent generation spectrum tailing at 870 nm.<sup>31</sup> In the CsPbI<sub>3</sub>, the band gap in the range of 1.67 eV.<sup>32</sup> A trend is that with the increase the size of A, i.e. from Cs<sup>+</sup>, to CH<sub>3</sub>NH<sub>3</sub><sup>+</sup> and NH<sub>2</sub>-CH=NH<sub>2</sub><sup>+</sup>, the value of the band gap is gradually decreased (Fig. 2). However, further increasing the size of A to CH<sub>3</sub>CH<sub>2</sub>NH<sub>2</sub> (EA), the perovskite CH<sub>3</sub>CH<sub>2</sub>NH<sub>3</sub>PbI<sub>3</sub> structure turns into orthorhombic symmetry ( $a = 8.7419(2)$  Å,  $b = 8.14745(10)$  Å, and  $c = 30.3096(6)$  Å), with a band gap of 2.2 eV.<sup>33</sup> According to the structural formation criterion, the volume threshold is CH<sub>3</sub>CH<sub>2</sub>NH<sub>2</sub> for the formation of cubic

APbI<sub>3</sub>. In this regard, there are quite limited number of molecules that can be applied in the A position for tuning the band structures. However, the change of M and X in AMX<sub>3</sub> can bring forth considerable changes of band gap, which will be discussed in the following sections.

### 2.2 The influence of M on the properties of perovskite

Lead is a kind of toxic element, the use of which is seriously restricted in European Union and some other countries.<sup>34</sup> This is thus the main reason for the development of lead-free or lead-less perovskite light absorbing materials. Sn in the same group as Pb is obviously the first choice as the alternative element. Ogomi et al. performed extensive investigations on the ratio between Sn and Pb in perovskite CH<sub>3</sub>NH<sub>3</sub>Sn<sub>1-x</sub>Pb<sub>x</sub>I<sub>3</sub> and found that the band gap can be tuned in 1.17-1.55 eV and thus the light absorption can be extended from visible to near infrared region (1060 nm).<sup>35</sup> A problem in the CH<sub>3</sub>NH<sub>3</sub>Sn<sub>1-x</sub>Pb<sub>x</sub>I<sub>3</sub> solar cell is that it's difficult to form uniform and dense absorber film over the device area. Therefore, the final efficiency achieved was only around 3%.<sup>35</sup>

The significant efficiency improvement in the tin-based perovskite solar cell was demonstrated by Hao et al.,<sup>36</sup> where CH<sub>3</sub>NH<sub>3</sub>SnI<sub>3</sub> was synthesized with a band gap of 1.3 eV. In this device, the light absorption can be extended to near IR region and the final PCE reached ~5%.<sup>37</sup> This is the first demonstration of the lead-free perovskite solar cells.

An interesting observation is that the energy gap in mixed tin and lead perovskites did not follow the Vegard's law, which is usually effective in the CuIn<sub>x</sub>Ga<sub>1-x</sub>Se<sub>2</sub>. For triiodide perovskite, CH<sub>3</sub>NH<sub>3</sub>Sn<sub>1-x</sub>Pb<sub>x</sub>I<sub>3</sub>, the two ends of the band gap in this work are measured to be 1.55 eV and 1.35 eV with  $x = 0$  and 1, while a band gap as small as 1.17 eV is obtained in CH<sub>3</sub>NH<sub>3</sub>Sn<sub>0.5</sub>Pb<sub>0.5</sub>I<sub>3</sub> and CH<sub>3</sub>NH<sub>3</sub>Sn<sub>0.75</sub>Pb<sub>0.25</sub>I<sub>3</sub>.<sup>36</sup> The device based on the CH<sub>3</sub>NH<sub>3</sub>SnI<sub>3</sub> and CH<sub>3</sub>NH<sub>3</sub>Sn<sub>0.25</sub>Pb<sub>0.75</sub>I<sub>3</sub> light absorbing materials exhibits PCEs of 5.44% and 7.37%, which are lower than the CH<sub>3</sub>NH<sub>3</sub>PbI<sub>3</sub> based device in the parallel investigations (8.31%). The main reason is again ascribed to the poor film quality and low surface coverage on the mesoporous TiO<sub>2</sub> nanoparticles.<sup>36</sup> This leads to low fill factor of the final devices. On the other hand, due to the downshifting of the

conduction band edge, there is always a decrease of open-circuit voltage in the Sn based perovskite when compared to the Pb equivalents.

### 2.3 The influence of X on the properties of perovskite

In the X position of perovskite, group VII elements, Cl, Br and I, are mostly applied candidates. The alternation in the element can bring forth great change in the band gap. In  $\text{CH}_3\text{NH}_3\text{PbX}_3$ , the band gaps are 3.11,<sup>38</sup> 2.22 and 1.51 eV for Cl, Br and I, respectively (Fig. 2).<sup>39</sup> It is also noted that tuning on X position in  $\text{CH}_3\text{NH}_3\text{PbX}_3$  (X = Cl, Br, I) cannot lead to band gap smaller than 1.51 eV. To generate appropriate band gap, researchers resort to altering two elements of M and X simultaneously. By partial replacement of the I with Br and complete replacement of Pb with Sn, Hao et al. observed that the band gap can be tuned to 1.30 and 2.15 eV in  $\text{CH}_3\text{NH}_3\text{SnI}_{3-x}\text{Br}_x$ .<sup>37</sup> The values are plotted in Fig. 3, which shows a rough linear relationship between I/Br ratio and the band gap values. In device investigation, when  $\text{CH}_3\text{NH}_3\text{SnI}_3$  is utilized as the light harvester, the photocurrent generation can be extended to 950 nm and the efficiency reaches 5.23%. The optimization on the ratio between I and Br shows that the

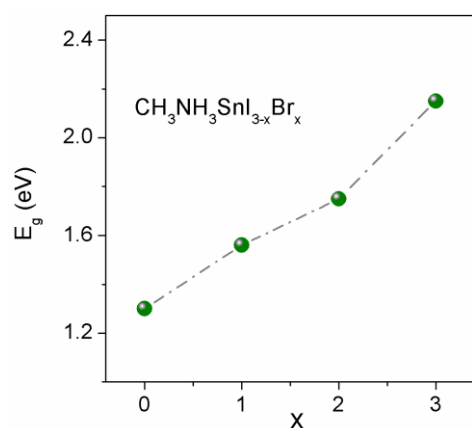


**Fig. 3** The relationship between I/Br ratio and band gap of  $\text{CH}_3\text{NH}_3\text{SnI}_{3-x}\text{Br}_x$ . Adapted and reprinted by permission from ref. 37. Copyright Macmillan Publishers Ltd (2014).

$\text{CH}_3\text{NH}_3\text{SnI}_3$  can generate PCE of 5.73%.

### 3. Device structures and fabrication

The device structures can be divided into three classes: (1) perovskite sensitized mesoporous architectures, (2) planar heterojunction configurations and (3) inverted structures, as depicted in Fig. 4.

In specific, the first type structure is similar to the solid-state DSSCs, where the perovskite absorber material fills the pores inside the  $\text{TiO}_2$  nanoparticle network and forms a cap layer on top. HTM is then coated on top of the perovskite film. It is finally completed by deposition of a layer of metal contact (Fig. 4a and 4b).<sup>24</sup> In this structure, the  $\text{TiO}_2$  as supporter and charge transport media, while the HTM is applied to transport the hole to the counter electrode.

Due to the chemical nature of the perovskite light absorbers, the loading of perovskite is also diverse. Initially, the attachment of perovskite was conducted by immersing pre-formed  $\text{TiO}_2$  nanoparticle network into the perovskite solution.<sup>20</sup> Apparently, the method is difficult to achieve high loading capacity. Later on, the infiltration of perovskite precursors was developed, in which  $\text{CH}_3\text{NH}_3\text{I}$  and  $\text{PbI}_2$  mixed

solution was spun coated onto the surface of mesoporous  $\text{TiO}_2$  nanoparticles; the spin coating drives the infiltration more efficiently.<sup>21</sup> To form denser perovskite layer on the  $\text{TiO}_2$  surface, a significant breakthrough was made by a two-step sequential deposition approach.<sup>24</sup> In this approach, the  $\text{PbI}_2$  was firstly infiltrated into the mesoporous  $\text{TiO}_2$  network, followed by immersing into  $\text{CH}_3\text{NH}_3\text{I}$  solution. The transformation to  $\text{CH}_3\text{NH}_3\text{PbI}_3$  is thus occurred at elevated temperature. By using this method, the efficiency can reach as high as 15% (Fig. 4c). On the ground of this device configuration, various nanostructured  $\text{TiO}_2$  and other wide band gap semiconducting oxide have been applied for the electron extraction materials. For example, to increase the charge transport, the mesoporous  $\text{TiO}_2$  nanoparticle network was replaced by the nanorod array, which has less grain boundaries that are believed to impede the charge transport.<sup>40, 41</sup> The use of ZnO as electron extraction material can generate efficiency of 11%.<sup>41</sup> In a recent review, Gao et al. have conducted extensive summarization on the use of various oxide supporters for the devices.<sup>42</sup>

Compared with the exciton diffusion length of some typical semiconducting polymers (around 10 nm), hybrid perovskite,  $\text{CH}_3\text{NH}_3\text{PbI}_{3-x}\text{Cl}_x$ , has an unusually long carrier diffusion length, more than  $1 \mu\text{m}$ .<sup>43</sup> This characteristic allows the construction of the devices in layered manner with enough thickness for sufficient light harvesting (Fig. 4d and 4e). To extract the electrons, similarly, n-type oxide material (such as  $\text{TiO}_2$  or ZnO) is usually adopted. The extraction of hole is achieved by HTM. The device is again completed by deposition of a layer of metal film. Two ways have been applied for the fabrication of perovskite layer for planar heterojunction solar cells. The co-evaporation method was initially developed by Snaith and co-workers,<sup>25</sup> in which the precursors such as  $\text{CH}_3\text{NH}_3\text{I}$  and  $\text{PbCl}_2$  are heated at respective temperatures. They thus reacted and deposited on the  $\text{TiO}_2$  compact layer. This approach is similar to the conventional vacuum deposition method for CIGS solar cells, in which different precursors were co-evaporated and deposited onto the substrate. Compared with the CIGS thin film, the deposition condition of perovskite absorber is simple and mild since there are only two types of precursor required for the target perovskite materials. This device fabrication method also leads to the final efficiency exceeding 15% (Fig. 4f).

A much more convenient way towards the planar heterojunction solar cells is through spin coating the mixed precursors on the compact layer of the device, which avoids the use of vacuum deposition apparatus. This feature generates broad interests in the device fabrication. In this method, hybrid perovskite  $\text{CH}_3\text{NH}_3\text{PbI}_{3-x}\text{Cl}_x$  was prepared by the reaction between  $\text{PbCl}_2$  and  $\text{CH}_3\text{NH}_3\text{I}$ , which allows the formation of uniform and compact films. In this fabrication method, it is noted that the reaction between  $\text{PbI}_2$  and  $\text{CH}_3\text{NH}_3\text{I}$  for the formation of  $\text{CH}_3\text{NH}_3\text{PbI}_3$  is quite fast and thus the film formability is difficult to control, usually forming discontinued nanocrystals on the compact layer of  $\text{TiO}_2$ . Therefore,  $\text{PbCl}_2$  and  $\text{CH}_3\text{NH}_3\text{I}$  are generally used as the precursors for the planar heterojunction perovskite solar cells. In the synthesis, annealing temperature and time are critical for the formation of high quality films for high performance solar cells. Dualeh and co-workers conducted detailed investigations on the dependence of the annealing condition for film morphology and composition.<sup>44</sup> It is found that annealing temperature below  $80 \text{ }^\circ\text{C}$  leads to much slow reaction and the complete transformation to perovskite requires  $>20 \text{ h}$ . On the other hand, when the temperature is higher than  $120 \text{ }^\circ\text{C}$ , the reaction becomes quite

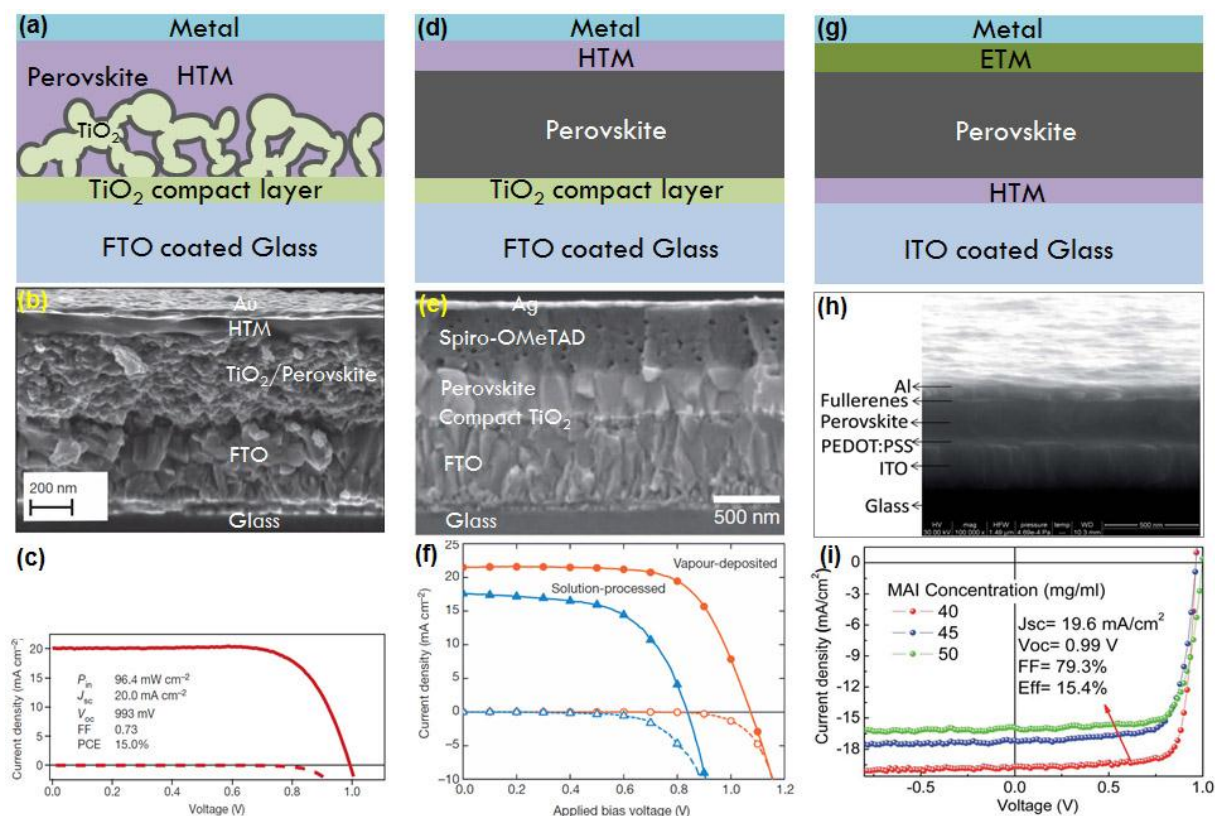


**Fig. 4** Device structures based on perovskite light absorbers. (a) A scheme of conventional mesoporous  $\text{TiO}_2$  network based perovskite solar cell, in which the perovskite is used as a sensitizer. (b) Scanning electron microscopy (SEM) image of the cross-section of the device. (c) A typical J-V curve of the mesoporous perovskite based solar cells. (b) and (c) are reprinted by permission from ref. 24. Copyright the Macmillan Publishers Ltd (2013). (d) Schematic illustration of a planar heterojunction based perovskite solar cell. (e) SEM image of the cross-section of the device. (f) A typical J-V curve of the mesoporous perovskite based solar cells. (e) and (f) are reprinted by permission from ref. 25. Copyright Macmillan Publishers Ltd (2013). (g) Schematic presentation of an inverted perovskite solar cell, in which hole transports to the ITO electrodes while electron transports to the metal electrode. (h) SEM image of the cross-section of the device. (i) A typical J-V curve of the mesoporous perovskite based solar cells. (h) and (i) are reproduced from ref. 48 with permission. Copyright the Royal Society of Chemistry (2014).

fast and can be finished in ten minutes or less, depending on the exact temperature. This high temperature reaction mostly gives rise to decomposition of perovskite to  $\text{PbI}_2$  and other species such as  $\text{CH}_3\text{NH}_3\text{I}$ ,  $\text{CH}_3\text{NH}_2$ , HI, etc.. Therefore, the annealing is usually conducted at  $\sim 100^\circ\text{C}$  for about 40 min. To obtain well-formed  $\text{CH}_3\text{NH}_3\text{PbI}_{3-x}\text{Cl}_x$  film by using  $\text{PbI}_2$  and  $\text{CH}_3\text{NH}_3\text{I}$  as precursors, Zhao et al. developed a method by adding  $\text{CH}_3\text{NH}_3\text{Cl}$  in the precursor solution, finally leading to excellent film formability and generating a PCE of 12%.<sup>45</sup> The results also show that the Cl in the final perovskite is not detectable. The loss of Cl is attributed to the sublimation of  $\text{CH}_3\text{NH}_3\text{Cl}$  or decomposition to other species and then left away.

A method by combining the vapour deposition and solution process was developed by Yang group, so-called vapour-assisted solution process (VASP).<sup>46</sup> In this method, the  $\text{PbI}_2$  was firstly deposited onto the compact layer of  $\text{TiO}_2$ . Afterwards,  $\text{CH}_3\text{NH}_3\text{I}$  was evaporated at  $150^\circ\text{C}$  and *in situ* reacted with pre-deposited  $\text{PbI}_2$  for 2 h in  $\text{N}_2$  gas atmosphere for the formation of final light absorber material. The reaction speed between vapour of  $\text{CH}_3\text{NH}_3\text{I}$  and  $\text{PbI}_2$  porous film can be tuned for good crystallinity and film formability of the final perovskite, which finally generated PCE of 12.1%.

In addition to the conventional device architectures, similar to the polymer solar cells,<sup>47</sup> the planar heterojunction perovskite solar cells can also be fabricated in an inverted manner (Fig. 4g and 4h).<sup>48</sup> In this perspective, the hole transfers to the ITO through an interlayer of HTM. Currently, the frequently used HTM is PEDOT:PSS which was also often used in polymer solar cells. The electron extraction materials are usually  $\text{C}_{60}$  derivatives. The advantages of this kind of structure are as follows. (1) The use of organic electron extraction materials to replace  $\text{TiO}_2$  compact layer can avoid the high temperature annealing process, enabling the temperature for device fabrication down to as low as  $100^\circ\text{C}$ . (2) The high cost sipro-OMeTAD can be replaced by other organic HTMs such as PEDOT:PSS. (3) It is more suitable for the fabrication of flexible devices. These characteristics attract increasing attention. Jeng et al. deposited various fullerene derivatives as the electron extraction materials on top of  $\text{CH}_3\text{NH}_3\text{PbI}_3$  for inverted structures.<sup>49</sup> However, the efficiency achieved was below 4%. Further improvement was conducted by introducing an interlayer between PCBM and metal contact,<sup>50</sup> and the optimization on the morphology of the films.<sup>51, 52</sup> However, the efficiencies are still moderate, below 10%. Most recently, Huang group elaborated the fabrication of

the perovskite films and electron transporting layer, a high efficiency of 15.4% and fill factor of 79.3% were obtained (Fig. 4i).<sup>48</sup>

#### 4. Operational principles of perovskite solar cells

The excellent photovoltaic performance is firstly attributed to the organometal perovskite light absorbing materials, which possess direct band structure with high light extinction coefficient.<sup>53</sup> This property allows the absorber film to be as thin as several hundred nanometres for enough light harvesting, while in traditional CIGS and silicon based solar cells the film thicknesses are usually at micrometre and hundreds of micrometre scale, respectively. In addition, photo-induced charge carrier generation in the organic-inorganic hybrid perovskite based device is quite fast, in picosecond timespan. The geminate recombination is, however, very slow, in tens of microseconds. These characteristics provide the possibility of obtaining efficient photocurrent generation efficiency for high short-circuit current density ( $J_{sc}$ ). On the other hand, compared with other thin film polycrystalline semiconductors, the perovskite absorber materials show low non-radiative recombination rate. This is evidenced by the small difference between the experiment open-circuit voltage ( $V_{oc}$ ) and the  $E_g/q$  values. The optimized device can reach  $E_g/q - V_{oc}$  values as low as 450 meV.<sup>27</sup> The high  $V_{oc}$  is the second factor that contributes to the high PCE. The high mobility is also a critical factor for the efficient photovoltaic energy conversions, which can generate high fill factor ( $FF$ ).

The diffusion length of charge carrier is an important parameter for assessing the recombination probabilities in the materials. Stranks, Edri and co-workers reported that the balanced electron and hole diffusion length of  $\text{CH}_3\text{NH}_3\text{PbI}_{3-x}\text{Cl}_x$  is over one micron which is about three times of the typical film thickness in the solar cell.<sup>54, 55</sup> This ensures the charges migrating to the interfaces before recombination. This attribute is especially significant for the fabrication of planar heterojunction solar devices. On the other hand, the diffusion length of  $\text{CH}_3\text{NH}_3\text{PbI}_3$  is only ~100 nm. Therefore, a mesoporous  $\text{TiO}_2$  nanoparticle network is necessary for transporting charges to the collecting electrode.

Furthermore, for perovskite solar cell with traditional DSSC-like structure, the charge transport is considered through the  $\text{TiO}_2$  nanoparticle network. The operational principle is just as the DSSC. In the device with planar heterojunction, or with insulating supporting scaffold, ambipolar carrier transport is regarded as the mechanism. Firstly, the exciton can quickly dissociate into free electrons and holes in the perovskite film and then the carrier transfer is conducted separately. The early study of the organometallic perovskite material reveals that at room temperature the exciton binding energy in  $\text{CH}_3\text{NH}_3\text{PbI}_3$  is in the range of 37-50 meV,<sup>56</sup> and the binding energy in mixed halide perovskite is 35-75 meV,<sup>57</sup> which is comparable to the room temperature thermal energy  $k_B T \sim 26$  meV. Thus, it is possible that the exciton can decouple to free charges (or unbound electron-hole pairs) at room temperature. The charge accumulation phenomenon within the perovskite film is confirmed by using the impedance spectroscopy.<sup>58</sup> This observation indicates that free charge carriers exist within the perovskite film. The cell configurations with insulating mesoporous alumina or without HTM layer can both work well which implies the ambipolar transport property of the perovskite material.<sup>23, 59</sup> Actually, in the so-called sensitized device structure with mesoporous  $\text{TiO}_2$  network, there is also continuous perovskite absorber. It is most likely that the

ambipolar charge transport mechanism is additionally at work. In this regard, it is suggested that there are indeed two complementary pathways for the electron transportation in the mesoporous configuration, namely through the perovskite film and through the titania network.<sup>60</sup> However, there is no conclusion which way is more efficient. To sum up, there are two possible ways for the generation of free charge in the solar cells. (1) Thermal energy is able to split the bound electron and hole pair. Actually, once the device is irradiated by the sunlight, the device temperature is instantaneously increased, the thermal energy  $k_B T$  will in turn gets increased for more efficient charge and hole separation. (2) Free charges are separated from the bound electron/hole pair at both the  $\text{TiO}_2$ /perovskite interface and the perovskite/HTM interface, which is proceeded at a timescale of picoseconds to nanoseconds.<sup>61</sup>

#### 5. Stability of perovskite solar cells

The instability of the perovskite solar cell comes from mainly the perovskite based light absorbers, which is highly sensitive to water (moisture). The decomposition of perovskite in presence of water is very fast, it can be finished in several minutes. The decomposed products are  $\text{CH}_3\text{NH}_3\text{I}$  and  $\text{PbI}_2$ . Therefore, to prevent the perovskite from water (moisture) could enhance the stability. Liu et al. used a HTM with long long alkyl chains, which can reduce the infiltration of water through the HTM layer to the perovskite.<sup>62</sup> In this work, the avoidance use of deliquescent additive also considerably improved durability. As a result, the stability is increased by two folds. In a most recent report, a 10  $\mu\text{m}$  thickness of carbon material was used as back contact which is believed to play a role as water-retaining layer.<sup>63</sup> The PCE of the device did not show decrease after storing in air for 1008 hours.

4-tert-butylpyridine (TBP) is an important additive in the conventional utilization of spiro-OMeTAD as HTM in perovskite solar cells. However, it is found TBP can react with perovskite, bringing forth device performance decay.<sup>64</sup> To minimize the corrosion effect on the perovskite, Li and coworkers incorporated montmorillonite as an interlayer in between perovskite and TBP to resist the reaction, rendering greatly improved device stability.<sup>64</sup>

The formation of perovskite  $\text{CH}_3\text{NH}_3\text{PbI}_3$  film is normally annealed at 100 °C for tens of minutes. Dualeh and co-workers found that, when the annealing temperature is higher than 120 °C, the perovskite starts to decompose into  $\text{PbI}_2$ ,  $\text{CH}_3\text{NH}_3\text{I}$  and  $\text{CH}_3\text{NH}_3\text{Cl}$ .<sup>44</sup> Once the temperature reach 300 °C, the perovskite decomposes into  $\text{PbI}_2$ ,  $\text{CH}_3\text{NH}_2$  and HI.

In addition to the water sensitivity, chemical reaction and thermal stability of perovskite, the instability of the device would also stem from  $\text{TiO}_2$  in some cases, owing to the non-stoichiometric  $\text{TiO}_2$  induced deep electron trap in the crystals. This phenomenon is especially notable in the inert atmosphere. This characteristic poses great challenge in the sealed devices to avoid the oxidation of dye or perovskite. Doping of Al into the  $\text{TiO}_2$  lattice can significantly reduce oxygen vacancy induced defect.<sup>65</sup>

The HTM also have influence on the device stability and efficiency. The conventional HTM is spiro-OMeTAD, it is important to oxidize the spiro-OMeTAD in order to improve the carrier mobility. However, the reversible oxidation reaction would also occur which decreases the device efficiency. To suppress the back reaction, Nguyen et al. synthesized dicationic salt of spiro-OMeTAD which can significantly improve the stability.<sup>66</sup> Compared with the conventional method, backward reaction due to the removal of oxygen (reaction between Li+

and oxygen to form  $\text{Li}_2\text{O}$ ) can be completely suppressed. It also is found that the introduction of  $\text{IrCp}^*\text{Cl}(\text{PyPyz})$  into the conventional spiro-OMeTAD can noticeably improve the device performance due to the reduced recombination rate.<sup>67</sup> The device stability is also increased, while the reason for the elongated stability remains uncovered.

While the stability has been improved to some extent, it is still far below the stringent requirement for long-term practical application. Therefore, further improvement is necessary in terms of both materials and device at laboratory and, more importantly, module scale.

## 6. Conclusions and outlook

Due to the achievable high efficiency, researchers with diverse backgrounds in physics, chemistry and materials science have contributed to the investigation of perovskite solar cells. The optimizations have been conducted on every single component such as the semiconducting oxide and polymer electron transporting layer, perovskite materials with different preparation methods, compositions, morphologies and light harvesting properties, organic and inorganic hole transporting materials as well as the metal contacts. With that, more and more understanding regarding the device has been accumulated. However, there are still some outstanding issues remaining unresolved, such as the chemical formation of the perovskite materials, working principles, materials processing and scalability, etc. We will analyse them in detail below. To solve the outstanding problems is actually the future directions for the development of organic-inorganic hybrid perovskite based solar cells.

**The chemical route for the formation of organic-inorganic hybrid perovskite.**  $\text{CH}_3\text{NH}_3\text{PbI}_{3-x}\text{Cl}_x$  possesses ultra-long diffusion length and can be used in both planar heterojunction and sensitized perovskite solar cells. The reaction kinetics between  $\text{PbCl}_2$  and  $\text{CH}_3\text{NH}_3\text{I}$  can be well controlled for the formation of uniform  $\text{CH}_3\text{NH}_3\text{PbI}_{3-x}\text{Cl}_x$  film. The annealing temperature and time are main factors that influence the final composition and morphology. It is repeatedly observed that the annealing process usually leads to significantly low content of chlorine in the final product, sometimes undetectable. In this regard, the hybrid compound is also called chlorine-doped perovskite. A common assumption is that the chlorine loss is through the sublimation or decomposition of  $\text{CH}_3\text{NH}_3\text{Cl}$ . However, so far there is no evidence for justifying this claim. This ambiguity arouses a couple questions regarding the reaction. What is the role played by the left chlorine-based compound in the reaction and film formation? Does it facilitate the formation of uniform film or change the physical property? In addition, the thermodynamic and kinetic natures of the reactions between  $\text{CH}_3\text{NH}_3\text{I}$  and  $\text{PbCl}_2$  or  $\text{PbI}_2$  are also remained uncovered.

**The carrier diffusion length in perovskite films.** It is generally recognized that the  $\text{CH}_3\text{NH}_3\text{PbI}_{3-x}\text{Cl}_x$  possesses much longer carrier diffusion length than  $\text{CH}_3\text{NH}_3\text{PbI}_3$ , 1  $\mu\text{m}$  vs. 100 nm. However, the reason for this difference is unclear. The physical property is associated with the chemical composition and the film quality in the measurement. The chlorine-doped perovskite can form dense, compact films with moderate grains, while the film quality of  $\text{CH}_3\text{NH}_3\text{PbI}_3$  perovskite is quite poor. The question whether the excellent diffusion length in the chlorine doped  $\text{CH}_3\text{NH}_3\text{PbI}_3$  perovskite is the intrinsic property or a result of high film quality is still unclear. To solve this problem, one needs to prepare comparable film of the two kinds of perovskites, and more importantly, to identify whether there

is still chlorine left in the final compound. However, so far there is no reliable way to make a clear conclusion.

**The materials of the organic-inorganic hybrid perovskite.** A great concern regarding the perovskite light absorption materials is the long-term stability. The chemical process is that the perovskite material binds with  $\text{H}_2\text{O}$  (moisture in air) and forms hydrated crystal. Therefore, the synthesis of perovskite is often conducted in dry condition such as glove box, which poses a great challenge in the large scale production. An alternative way to extend the lifetime is to develop stringent sealing technique. However, this will increase the cost of the solar cell fabrications and installations. In addition to the stability, the toxic element Pb is also a serious problem. The most possible approach is to replace Pb by Sn. However, as discussed above, the Sn based perovskites exhibit much poorer device performance. The improvement on the efficiency requires the understanding of the optical and electronic properties, exploration of appropriate device structures, tuning of internal electron dynamics and engineering of the corresponding interfacial properties.

**The high cost hole transporting materials.** To date, the high efficiency is generally achieved by using spiro-OMeTAD or its derivatives as the HTM.<sup>23-25, 68</sup> In the device, a considerably thick layer of spiro-OMeTAD is often used. Therefore, to find a low-cost and high-efficiency HTM is a

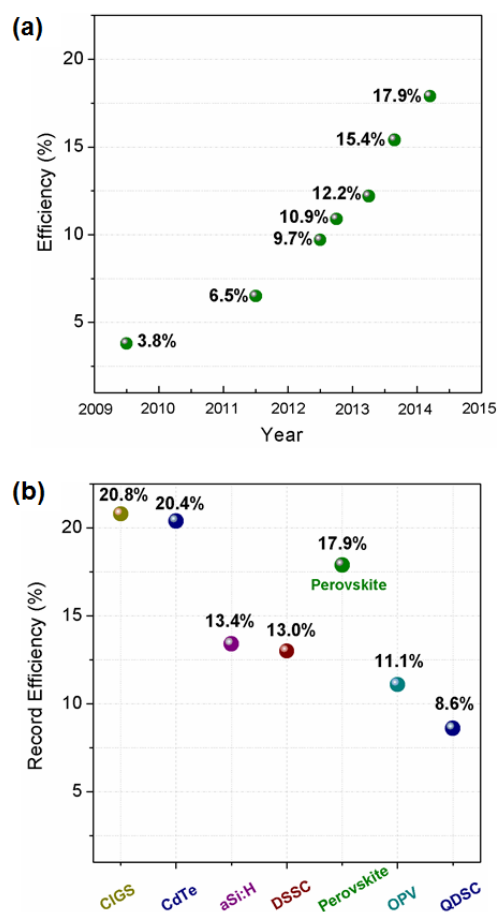


**Fig. 5** (a) Partial landmark efficiencies of the perovskite solar cells (ref. 2, 20, 21, 22, 23, 25 and 54); others are referred in the main text. (b) The record efficiencies of the solar cells based on CIGS, CdTe, aSi:H, DSSC, perovskite, OPV and QDSC (data from ref. 2, updated to June 2014).

significant task for future applications. To date, a few studies have involved into the exploration of low-cost alternatives, such as those based on semiconducting polymer,<sup>69, 70</sup> inorganic CuI, etc.<sup>71</sup> However, the performance is significantly lower than the traditional spiro-OMeTAD. Deposition of metal directly on the perovskite which forms a Schottky barrier can also complete the device.<sup>59, 72, 73</sup> Though the fabrication becomes simpler and avoids the use of HTM, the efficiency is essentially lower than the standard spiro-OMeTAD equivalents.

Regardless the outstanding issues in perovskite solar cells, the fast growing efficiencies are undoubtedly great encouragement for further investigation (Fig. 5a). An estimation shows that the limit efficiency of perovskite solar cell is around 20%, with  $J_{sc} = 22 \text{ mA cm}^{-2}$ ,  $V_{oc} = 1.1 \text{ V}$  and  $FF = 0.8$ .<sup>27</sup> This value is close to the thin film CIGS and CdTe solar cells (Fig. 5b). The use of multi-layered perovskites with different band gaps stacking in appropriate manner is expected to be able to further increase the energy conversion efficiency. On the other hand, the combination between perovskite solar cell with high efficiency silicon and CIGS based solar cells to create tandem device structure is capable of generating 30% efficiency in the integrated device. More importantly, the high PCEs (>15%) have been reported by a number of research groups. This suggests that the fabrication of high quality perovskite solar device is fairly reliable and reproducible.

Through there are some comments on the perovskite solar cells,<sup>74-76</sup> there has been no detailed analysis on the price and potential of the solar cells. Actually, perovskite solar cells make an excellent combination between the advantage of the high energy conversion efficiencies achieved in silicon, CIGS and CdTe solar cells and the cost-effective solution processing in the third generation DSSCs and OPVs. Suppose that the device is stable enough, it is predicted that perovskite solar modules will cost about \$0.30 per Watt peak,<sup>77</sup> which is significantly lower than those of silicon (\$1 per watt in 2013), CIGS (\$0.55 per Watt estimated by Manz)<sup>78</sup> and CdTe (\$0.67 per Watt from First Solar) solar modules, demonstrating the competitiveness of perovskite solar cells. Obviously, the long-term stability of the perovskite has to be improved to a considerable extent, while it is difficult to predict when it can be well-installed for residence system. In the near future, a rational assumption is that the price of silicon solar cell will be continually decreased. As evaluated by Bloomberg (New Energy Finance & PV.energytrend.com), the price of silicon will be decreased to \$0.36 per Watt in 2014. Therefore, considering the price competitiveness, a variety of solar cells will coexist in the market. Since each of the devices possesses its own nature, the application field will be diverse. Obviously, the third-generation solar cells will be especially applicable for the build-integrated colourful and semi-transparent photovoltaics, while the silicon solar cell and second-generation thin film solar cells are more feasible in solar electricity stations and rooftop. With that, an optimistic prediction is that the reliance on the fossil fuels for electricity will be gradually and considerably alleviated.

## Acknowledgements

This work was substantially supported by a grant from the Research Grants Council of the Hong Kong Special Administrative Region, China, under Theme-based Research Scheme through Project No. T23-407/13-N. The authors also acknowledge the financial support from the CUHK Group Research Scheme and CUHK Focused Scheme B Grant

“Centre for Solar Energy Research”, CUHK direct grant 4053068 and 4053012.

## Notes and references

Department of Physics, The Chinese University of Hong Kong, Shatin, Hong Kong, China. Fax: 852- 2603 5204; Tel: 852-3943 6278; E-mail: taochen@phy.cuhk.edu.hk (T. C.); xdxiao@phy.cuhk.edu.hk (X. D. X).

† Footnotes should appear here. These might include comments relevant to but not central to the matter under discussion, limited experimental and spectral data, and crystallographic data.

Electronic Supplementary Information (ESI) available: [details of any supplementary information available should be included here]. See DOI: 10.1039/b000000x/

- 1 M. Gratzel, *Nature*, 2001, **414**, 338.
- 2 M. A. Green, K. Emery, Y. Hishikawa, W. Warta and E. D. Dunlop, *Prog. Photovolt. Res. Appl.*, 2014, **22**, 701.
- 3 B. Oregan and M. Gratzel, *Nature*, 1991, **353**, 737.
- 4 C. W. Tang, *Appl. Phys. Lett.*, 1986, **48**, 183.
- 5 G. Yu, J. Gao, J. C. Hummelen, F. Wudl and A. J. Heeger, *Science*, 1995, **270**, 1789.
- 6 S. Chang, Q. Li, X. Xiao, K. Y. Wong and T. Chen, *Energy Environ. Sci.*, 2012, 9444.
- 7 B. Wang, S. Chang, L. T. L. Lee, S. Zheng, K. Y. Wong, Q. Li, X. Xiao and T. Chen, *Acs Appl. Mater. & Interfaces*, 2013, **5**, 8289.
- 8 L. T. L. Lee, J. He, B. Wang, Y. Ma, K. Y. Wong, Q. Li, X. Xiao and T. Chen, *Sci. Rep.*, 2014, **4**.
- 9 A. Hagfeldt, G. Boschloo, L. C. Sun, L. Kloo and H. Pettersson, *Chem. Rev.*, 2010, **110**, 6595.
- 10 B. C. Thompson and J. M. J. Frechet, *Angew. Chem. -In. Ed.*, 2008, **47**, 58.
- 11 H. A. Atwater and A. Polman, *Nature Mater.*, 2010, **9**, 205.
- 12 A. Yella, H. W. Lee, H. N. Tsao, C. Y. Yi, A. K. Chandiran, M. K. Nazeeruddin, E. W. G. Diau, C. Y. Yeh, S. M. Zakeeruddin and M. Gratzel, *Science*, 2011, **334**, 629.
- 13 S. Mathew, A. Yella, P. Gao, R. Humphry-Baker, B. F. E. Curchod, N. Ashari-Astani, I. Tavernelli, U. Rothlisberger, M. K. Nazeeruddin and M. Gratzel, *Nature Chem.*, 2014, **6**, 242.
- 14 Q. Yu, Y. Wang, Z. Yi, N. Zu, J. Zhang, M. Zhang and P. Wang, *Acs Nano*, 2010, **4**, 6032.
- 15 P. Maraghechi, A. J. Labelle, A. R. Kirmani, X. Lan, M. M. Adachi, S. M. Thon, S. Hoogland, A. Lee, Z. Ning, A. Fischer, A. Amassian and E. H. Sargent, *Acs Nano*, 2013, **7**, 6111.
- 16 P. V. Kamat, *J. Phys. Chem. Lett.*, 2013, **4**, 908.
- 17 Z. He, C. Zhong, S. Su, M. Xu, H. Wu and Y. Cao, *Nature Photon.*, 2012, **6**, 591.
- 18 Z. He, C. Zhong, X. Huang, W.-Y. Wong, H. Wu, L. Chen, S. Su and Y. Cao, *Adv. Mater.*, 2011, **23**, 4636.
- 19 R. F. Service, *Science*, 2011, **332**, 293.
- 20 A. Kojima, K. Teshima, Y. Shirai and T. Miyasaka, *J. Am. Chem. Soc.*, 2009, **131**, 6050.
- 21 J. H. Im, C. R. Lee, J. W. Lee, S. W. Park and N. G. Park, *Nanoscale*, 2011, **3**, 4088.
- 22 H. S. Kim, C. R. Lee, J. H. Im, K. B. Lee, T. Moehl, A. Marchioro, S. J. Moon, R. Humphry-Baker, J. H. Yum, J. E. Moser, M. Gratzel and N. G. Park, *Sci. Rep.*, 2012, **2**.

- 23 M. M. Lee, J. Teuscher, T. Miyasaka, T. N. Murakami and H. J. Snaith, *Science*, 2012, **338**, 643.
- 24 J. Burschka, N. Pellet, S. J. Moon, R. Humphry-Baker, P. Gao, M. K. Nazeeruddin and M. Grätzel, *Nature*, 2013, **499**, 316.
- 25 M. Z. Liu, M. B. Johnston and H. J. Snaith, *Nature*, 2013, **501**, 395.
- 26 J. Calabrese, N. L. Jones, R. L. Harlow, N. Herron, D. L. Thorn and Y. Wang, *J. Am. Chem. Soc.*, 1991, **113**, 2328.
- 27 H. J. Snaith, *J. Phys. Chem. Lett.*, 2013, **4**, 3623.
- 28 T. Umebayashi, K. Asai, T. Kondo and A. Nakao, *Phys. Rev. B*, 2003, **67**, 155405.
- 29 E. Mosconi, A. Amat, M. K. Nazeeruddin, M. Grätzel and F. De Angelis, *J. Phys. Chem. C*, 2013, **117**, 13902.
- 30 W. Shockley and H. J. Queisser, *J. Appl. Phys.*, 1961, **32**, 510.
- 31 S. Pang, H. Hu, J. Zhang, S. Lv, Y. Yu, F. Wei, T. Qin, H. Xu, Z. Liu and G. Cui, *Chem. Mater.*, 2014, **26**, 1485.
- 32 C. C. Stoumpos, C. D. Malliakas and M. G. Kanatzidis, *Inorg. Chem.*, 2013, **52**, 9019.
- 33 J.-H. Im, J. Chung, S.-J. Kim and N.-G. Park, *Nanoscale Res. Lett.*, 2012, **7**, 353.
- 34 Restriction of the use of certain hazardous substances (RoHS), Directive 2011/65/EU.
- 35 Y. Ogomi, A. Morita, S. Tsukamoto, T. Saitho, N. Fujikawa, Q. Shen, T. Toyoda, K. Yoshino, S. S. Pandey, T. Ma and S. Hayase, *J. Phys. Chem. Lett.*, 2014, **5**, 1004.
- 36 F. Hao, C. C. Stoumpos, R. P. H. Chang and M. G. Kanatzidis, *J. Am. Chem. Soc.*, 2014, **136**, 8094.
- 37 F. Hao, C. C. Stoumpos, D. H. Cao, R. P. H. Chang and M. G. Kanatzidis, *Nature Photon.*, 2014, **8**, 489.
- 38 N. Kitazawa, Y. Watanabe and Y. Nakamura, *J. Mater. Sci.*, 2002, **37**, 3585.
- 39 J. H. Noh, S. H. Im, J. H. Heo, T. N. Mandal and S. I. Seok, *Nano Lett.*, 2013, **13**, 1764.
- 40 D. Bi, G. Boschloo, S. Schwarzmueller, L. Yang, E. M. J. Johansson and A. Hagfeldt, *Nanoscale*, 2013, **5**, 11686.
- 41 D.-Y. Son, J.-H. Im, H.-S. Kim and N.-G. Park, *J. Phys. Chem. C*, 2014.
- 42 P. Gao, M. Grätzel and M. K. Nazeeruddin, *Energy Environ. Sci.*, 2014.
- 43 G. Xing, N. Mathews, S. Sun, S. S. Lim, Y. M. Lam, M. Grätzel, S. Mhaisalkar and T. C. Sum, *Science*, 2013, **342**, 344.
- 44 A. Dualeh, N. T. A. Reddy, T. Moehl, P. Gao, M. K. Nazeeruddin and M. Grätzel, *Adv. Funct. Mater.*, 2014, **24**, 3250.
- 45 Y. Zhao and K. Zhu, *J. Phys. Chem. C*, 2014, **118**, 9412.
- 46 Q. Chen, H. Zhou, Z. Hong, S. Luo, H.-S. Duan, H.-H. Wang, Y. Liu, G. Li and Y. Yang, *J. Am. Chem. Soc.*, 2013, **136**, 622.
- 47 S. K. Hau, H. L. Yip and A. K. Y. Jen, *Polymer Rev.*, 2010, **50**, 474.
- 48 Z. Xiao, C. Bi, Y. Shao, Q. Dong, Q. Wang, Y. Yuan, C. Wang, Y. Gao and J. Huang, *Energy Environ. Sci.*, 2014.
- 49 J.-Y. Jeng, Y.-F. Chiang, M.-H. Lee, S.-R. Peng, T.-F. Guo, P. Chen and T.-C. Wen, *Adv. Mater.*, 2013, **25**, 3727.
- 50 P. Docampo, J. M. Ball, M. Darwich, G. E. Eperon and H. J. Snaith, *Nat. Commun.*, 2013, **4**.
- 51 H.-B. Kim, H. Choi, J. Jeong, S. Kim, B. Walker, S. Song and J. Y. Kim, *Nanoscale*, 2014, **6**, 6679.
- 52 S. Sun, T. Salim, N. Mathews, M. Duchamp, C. Boothroyd, G. Xing, T. C. Sum and Y. M. Lam, *Energy Environ. Sci.*, 2014, **7**, 399.
- 53 P. Umari, E. Mosconi and F. De Angelis, *Sci. Rep.*, 2014, **4**.
- 54 S. D. Stranks, G. E. Eperon, G. Grancini, C. Menelaou, M. J. P. Alcocer, T. Leijtens, L. M. Herz, A. Petrozza and H. J. Snaith, *Science*, 2013, **342**, 341.
- 55 E. Edri, S. Kirmayer, A. Henning, S. Mukhopadhyay, K. Gartsman, Y. Rosenwaks, G. Hodes and D. Cahen, *Nano Lett.*, 2014, **14**, 1000.
- 56 K. Tanaka, T. Takahashi, T. Ban, T. Kondo, K. Uchida and N. Miura, *Solid State Commun.*, 2003, **127**, 619.
- 57 V. D'Innocenzo, G. Grancini, M. J. P. Alcocer, A. R. S. Kandada, S. D. Stranks, M. M. Lee, G. Lanzani, H. J. Snaith and A. Petrozza, *Nature Commun.*, 2014, **5**.
- 58 H. S. Kim, I. Mora-Sero, V. Gonzalez-Pedro, F. Fabregat-Santiago, E. J. Juarez-Perez, N. G. Park and J. Bisquert, *Nat. Commun.*, 2013, **4**.
- 59 L. Etgar, P. Gao, Z. Xue, Q. Peng, A. K. Chandiran, B. Liu, M. K. Nazeeruddin and M. Grätzel, *J. Am. Chem. Soc.*, 2012, **134**, 17396.
- 60 V. Rofailo, S. Colella, G. Lerario, L. De Marco, A. Rizzo, A. Listorti and G. Gigli, *Energy Environ. Sci.*, 2014, **7**, 1889.
- 61 A. Marchioro, J. Teuscher, D. Friedrich, M. Kunst, R. van de Krol, T. Moehl, M. Grätzel and J.-E. Moser, *Nature Photon.*, 2014, **8**, 250.
- 62 J. Liu, Y. Wu, C. Qin, X. Yang, T. Yasuda, A. Islam, K. Zhang, W. Peng, W. Chen and L. Han, *Energy Environ. Sci.*, 2014, **7**, 2963.
- 63 A. Mei, X. Li, L. Liu, Z. Ku, T. Liu, Y. Rong, M. Xu, M. Hu, J. Chen, Y. Yang, M. Grätzel and H. Han, *Science*, 2014, **345**, 295.
- 64 W. Li, H. Dong, L. Wang, N. Li, X. Guo, J. Li and Y. Qiu, *J. Mater. Chem. A*, 2014, **2**, 13587.
- 65 S. K. Pathak, A. Abate, P. Ruckdeschel, B. Roose, K. C. Gödel, Y. Vaynzof, A. Santhala, S.-I. Watanabe, D. J. Hollman, N. Noel, A. Sepe, U. Wiesner, R. Friend, H. J. Snaith and U. Steiner, *Adv. Funct. Mater.*, 2014, n/a.
- 66 W. H. Nguyen, C. D. Bailie, E. L. Unger and M. D. McGehee, *J. Am. Chem. Soc.*, 2014, **136**, 10996.
- 67 L. Badia, E. Mas-Marzá, R. S. Sánchez, E. M. Barea, J. Bisquert and I. Mora-Seró, *APL Mater.*, 2014, **2**.
- 68 N. J. Jeon, H. G. Lee, Y. C. Kim, J. Seo, J. H. Noh, J. Lee and S. I. Seok, *J. Am. Chem. Soc.*, 2014, **136**, 7837.
- 69 F. Di Giacomo, S. Rizza, F. Matteocci, A. D'Epifanio, S. Licoccia, T. M. Brown and A. Di Carlo, *J. Power Sources*, 2014, **251**, 152.
- 70 B. Cai, Y. D. Xing, Z. Yang, W. H. Zhang and J. S. Qiu, *Energy Environ. Sci.*, 2013, **6**, 1480.
- 71 J. A. Christians, R. C. M. Fung and P. V. Kamat, *J. Am. Chem. Soc.*, 2013, **136**, 758.
- 72 W. A. Laban and L. Etgar, *Energy Environ. Sci.*, 2013, **6**, 3249.
- 73 J. Shi, J. Dong, S. Lv, Y. Xu, L. Zhu, J. Xiao, X. Xu, H. Wu, D. Li, Y. Luo and Q. Meng, *Appl. Phys. Lett.*, 2014, **104**.
- 74 M. He, D. Zheng, M. Wang, C. Lin and Z. Lin, *J. Mater. Chem. A*, 2014, **2**, 5994.
- 75 S. Kazim, M. K. Nazeeruddin, M. Grätzel and S. Ahmad, *Angew. Chem. - Int. Ed.*, 2014, **53**, 2812.
- 76 G. Hodes and D. Cahen, *Nat. Photon.*, 2014, **8**, 87.
- 77 <http://www.rsc.org/chemistryworld/2013/04/cheap-perovskite-solar-cells-al2o3>.
- 78 Manzhong, [http://www.pv-magazine.com/news/details/beitrag/manzhong-reaches-146-cigs-panel-efficiency\\_100008373/#axzz36fhPNZ77](http://www.pv-magazine.com/news/details/beitrag/manzhong-reaches-146-cigs-panel-efficiency_100008373/#axzz36fhPNZ77).